

Effect of control route on the unstart/restart characteristics of an over-under TBCC inlet

Nan Li^{1,2a}, Juntao Chang^{*2}, Jingfeng Tang^{2b}, Daren Yu^{2c}, Wen Bao^{2d} and Yanping Song^{2e}

¹Science and Technology on Scramjet Laboratory, Hypervelocity Aerodynamics Institute of CARDC, Sichuan, Mianyang 621000, People's Republic of China

²Harbin Institute of Technology, Harbin, Heilongjiang 150001, People's Republic of China

(Received September 25, 2017, Revised November 21, 2017, Accepted December 27, 2017)

Abstract. Numerical simulations have been conducted to study the unstart/restart characteristics of an over-under turbine-based combined-cycle propulsion system (TBCC) inlet during the inlet transition phase. A dual-solution area exists according to the Kantrowitz theory, in which the inlet states may be different even with the same input parameters. The entire transition process was divided into five stages and the unstart/restart hysteresis loop for each stage was also obtained. These loops construct a hysteresis surface which separates the operating space of the engine into three parts: in which a) inlet can maintain a started state; b) inlet keeps an unstarted state; c) inlet state depends on its initial state. During the transition, the operation of the engine follows a certain order with different backpressures and splitter angles, namely control route, which may result in disparate inlet states. Nine control routes with different backpressures and transition stages were designed to illuminate the route-dependent behavior of the inlet. The control routes operating towards the unstart boundary can make the inlet transit from a started state into an unstarted one. But operating backward the same route cannot make the inlet restart, additional effort should be made.

Keywords: inlet mode transition; unstart/restart hysteresis; control route; route-dependent

1. Introduction

Inlet unstart is an inevitable problem when studying supersonic/hypersonic airbreathing propulsion system. In previous flight tests, inlet unstart took place frequently and many of them ended in failure unfortunately. In 2011, the X-51A experienced a terrible inlet unstart when the engine attempted to transit to JP7 fuel operation. After detecting the unstart, the aircraft took actions to restart but attempts proved unsuccessful (Norris 2011). Flight test of a dual-mode scramjet engine was conducted by CIAM in 1998 under contract from NASA. Unfortunately, the

*Corresponding author, Professor, E-mail: changjuntao@hit.edu.cn

^aPh.D. Student, E-mail: 14B902020@hit.edu.cn

^bProfessor, E-mail: tangjingf@hit.edu.cn

^cProfessor, E-mail: yudaren@hit.edu.cn

^dProfessor, E-mail: baowen@hit.edu.cn

^eProfessor, E-mail: songyanping@hit.edu.cn

flight-test results showed that the inlet unstated when the fuel was first injected and remained unstated, due to over fueling (Volland and Auslender 1999). Also, in the flight test of HyCAUSE, the unstart phenomenon emerged periodically and partially contributed to the absence of hydrogen combustion in the combustor (Walker *et al.* 2008). Since the importance of the inlet unstart, many studies have been conducted to study the mechanism and the influence of different parameters on inlet start/unstart. Recent correlational researches have been summarized by Chang *et al.* (2017).

An essential part of this study is to construct an operating space for TBCC inlet. The isentropic and Kantrowitz theory have already given a criterion to enforce (Kantrowitz and Donaldson 1945). Above the Kantrowitz line, the inlet can achieve self-start, while below the isentrope line, a large compression area ratio stops the inlet from starting due to the insufficient mass flow. While in the region bounded by the two curves, namely dual-solution area, both started and unstated states are possible. According to the dynamical system theories, the inlet with a configuration in this region has a property of bistability. For this system, the operating states with different control routes may be disparate even with the same input (Cui *et al.* 2011). For the fixed geometry inlet with a designed contraction ratio, one should only concern the effect of Mach number, the angle of attack (AOA) and the backpressure when controls the engine. While for the TBCC inlet, the contraction ratio varies during the inlet transition process. Besides, the inlet unstart is not only induced by the contraction ratio, AOA or Mach number, the backpressure also contributes to the inlet unstart process. Multi-parameter coupling exists during the inlet transition, which brings a great challenge for control purpose.

A major goal of the current work is to verify the effect of the control route on the unstart/restart characteristics of the TBCC inlet. The switching procedure between the two engines is called mode transition. The inlet should provide the airflow with proper parameters for combined-cycle propulsion system to ensure a smooth transition from turbojet to ramjet engine. Especially, smooth and stable mode transition is essential for the feasibility of the combined-cycle propulsion system (Cui *et al.* 2011). One of the concerns for the mode transition is that both the low-speed (LS) inlet and the high-speed (HS) inlet are operating simultaneously, but in an off-design condition. To ensure a smooth transition, we should pay close attention to the potential of the inlet unstart during the mode transition. In fact, there is little information in the literatures that demonstrates the unstart/restart characteristics during the transition phase. Due to the route-dependent behavior, namely hysteresis, the inlet is unable to restart along the same control route which makes it unstart. Besides, the hysteresis phenomenon is very common in ramjet/scramjet (Kuzmin 2015a, b, 2016, Cui *et al.* 2012, 2014). Cui and his colleagues (Cui *et al.* 2011) have analyzed the loops-coupled hysteresis phenomenon occurred in the CIAM test, a neglect of the loops-coupled hysteresis phenomenon has given rise to the error detection of inlet start/unstart. From the point of engine operation, the ramjet/scramjet needs to be ignited to gain enough thrust during the transition phase. Once the inlet unstart occurs, the thrust will be declined sharply. Usually a control method, such as reducing the fuel supply, can make the inlet restart. Due to the operating space and the hysteresis behavior of the system, different control routes will result in disparate inlet states. The engine should be operated by rules.

For improving the understanding of the flow instability in the TBCC inlet during the transition phase, the unstart/restart characteristics should be analyzed. Meanwhile, to maintain a good performance of the engine, the effect of the control routes should also be concerned. Firstly, the present study is undertaken to provide the flow characteristics of the inlet at different transition stages by numerical simulation. The unstart/restart boundary of each stage is given based on the relationship between the mass flow rate and the pressure ratio. The differences between the two

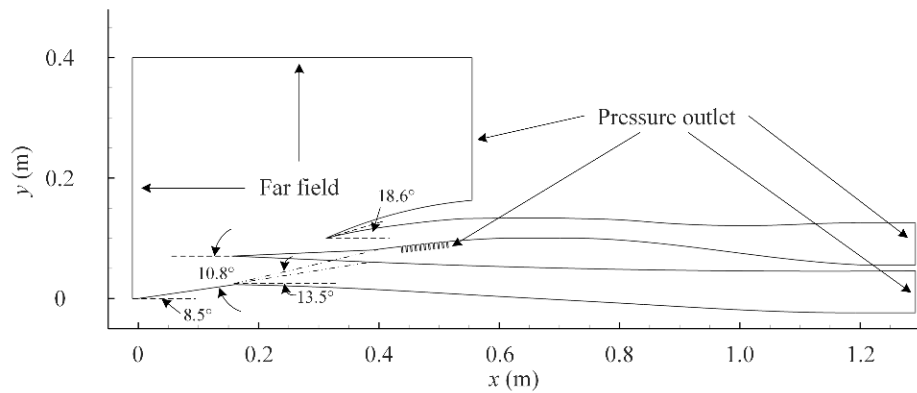


Fig. 1 Computational domain and boundary conditions of the over-under TBCC inlet model (Wang, Zhuang *et al.* 2011)

boundaries construct the hysteresis loop. And these loops consist a hysteresis surface, which divides the operating space of the engine into three parts. Then, nine control routes were designed to demonstrate the route-dependent behavior of the inlet unstart/restart transition.

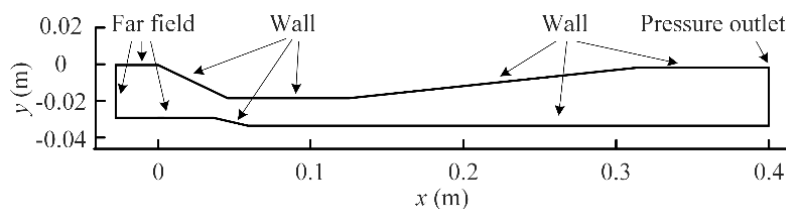
2. Model setup and numerical approach validation

2.1 Inlet model

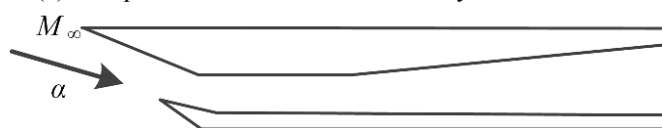
The inlet model is shown in Fig. 1. The TBCC inlet contains two ducts: LS duct for the turbine engine and HS duct for the ramjet engine, which share a same external compression surface. The first deflection angle of the compression surface (external compression surface) is 8.5° . The second deflection angle of the compression surface for the ramjet is 5° . The deflection angle of the LS duct and HS duct cowl is 10.8° and 5.1° , respectively. The HS inlet was designed for a shock-on-lip Mach number of 4. The LS inlet is opened from takeoff to Mach 2. Above Mach 2, the splitter will be closed so that flow is being supplied only to the ramjet engine. In this simulation, M_∞ , p_∞ , T_∞ and unite Reynolds number were set as 2.0 (2.5), 22700 Pa, 216.7 K and $4e+7$ /m.

2.2 Numerical method and validation

Two-dimensional compressible Reynolds-averaged Navier-Stokes (RANS) simulations have been performed with the help of commercial software FLUENT. Its accuracy has been validated in many references (Taha *et al.* 2001, Fu *et al.* 2016). The $k-\omega$ Shear Stress Transport (SST) turbulence model developed by Menter (1994) was selected to simulate the wall-bounded turbulent flow, which has shown a great advantage in predicting the adverse pressure gradient flows (Häberle and Gülhan 2008, Raj and Venkatasubbaiah 2012). The compressibility correlation has been taken into consideration and the Wilcox correlation model was used (Wilcox 1994). To provide exact resolution of shock discontinuities, the Advection Upstream Splitting Method (AUSM) was employed for the approximation of the convective flux splitting and the governing equations were discretized by the second-order upwind method. The density based solver with an implicit time-marching algorithm was used. The fluid was considered to be a single-specie,



(a) Computational domain and boundary conditions



(b) A sketch of the similar inlet model

Fig. 2 Test model used by Herrmann and Koschel (2002)

calorically perfect air. The piecewise-polynomial method was selected to compute specific heat while viscosity was solved using Sutherland's formula.

2.3 Numerical approach validation and grid sensitivity analysis

For the test model shown in Fig. 2, the experimental results of Herrmann and Koschel (2002) have been selected to validate the numerical method and confirm the grid resolution. As shown in Fig. 2(a), three types of boundary condition were used in the computations. To achieve similar flow conditions, the angle of incidence (α) of the model was changed to 10° according to the former ramp geometry as shown in Fig. 2(b). In this validation case, M_∞ , p_∞ and T_∞ were set as 2.41, 36364 Pa and 141.1 K, respectively (Herrmann and Koschel 2002). To ensure that the boundary layers, shock interactions and separation zones are properly resolved, the height of the lowest grids near wall are set as $5e-5$ m and a value of y^+ below 3 is realized for the main portion of the first layer of near wall grids.

In Fig. 3, we report the non-dimensionalized wall pressure distributions obtained by the three grids ($5e-4$ m, $2e-4$ m, $1e-4$ m) compared with the experimental results. The calculated pressure distributions agree well with the experimental values and the results predicted by the three grids are almost identical. The flow structures of the inlet/isolator obtained by the fine grid ($2e-4$ m) are shown in Fig. 2 along with the experimental Schlieren images. As it can be seen, the results are generally consistent with the experimental ones. The shock wave pattern, the separation and the approximate boundary-layer thickness of the Schlieren picture are also present in the simulation results. Simulation results capture the separated bubble induced by the shock/turbulent boundary layer interactions correctly, but little difference exists. It loses the details of the shedding vortices at the shear layer. The separated shock in the numerical simulation is weaker than what was observed in the experiment. As shown in Fig. 2(a), the numerically predicted separation induced shock is downstream of that in the experiment and it makes the pressure distribution a little different from the experiment one. The same phenomenon was reported by Chang *et al.* (2009). The reason for the discrepancy was probably the differences between the experimental and computational conditions that were the uniformity of the inflow condition and the three-dimensional effect, or the deficiency of the eddy viscosity hypothesis (Chang *et al.* 2009). For the unstart case, the pressure at the exit was set a value the same with that of the experiment. Fig. 2(b)

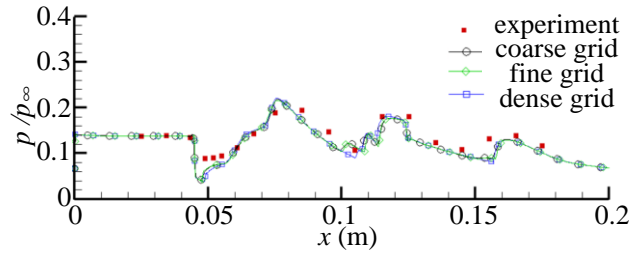


Fig. 1 Distributions of the static pressure along the bottom wall

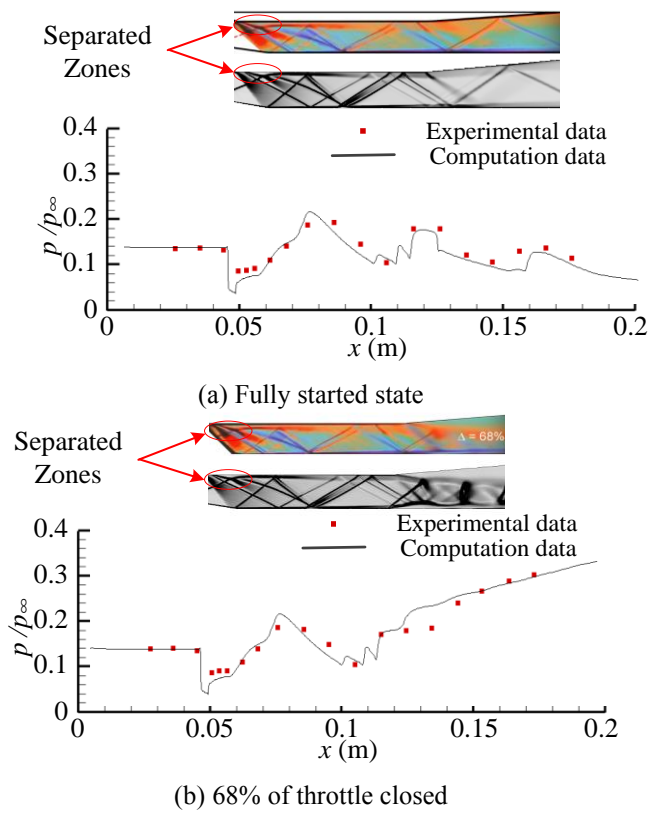
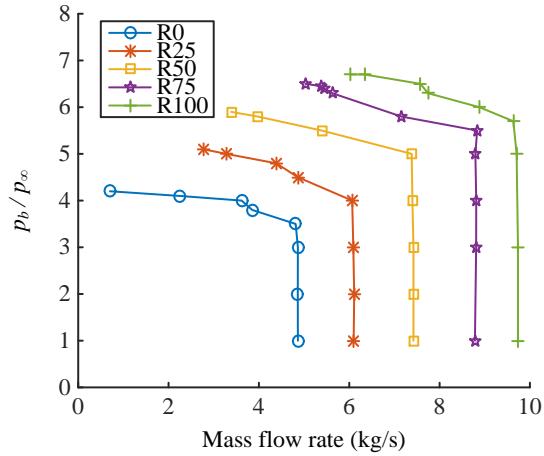


Fig. 2 Experimental/numerical Schlieren images and distributions of the static pressure along the bottom wall

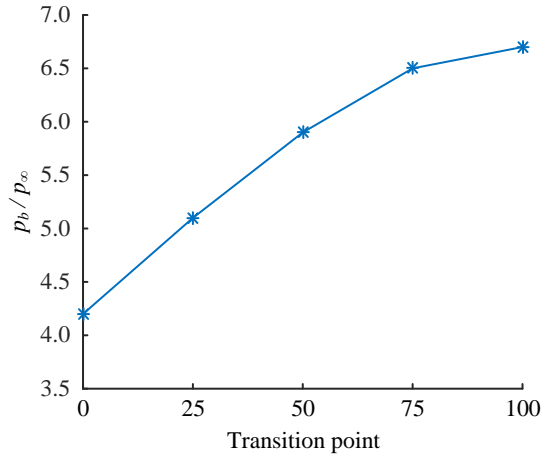
Table 1 Definition of different transition stages in the simulations

Transition phase	R0	R25	R50	R75	R100
Inlet state	LS inlet is opened completely	LS inlet closes 25%	LS inlet closes 50%	LS inlet closes 75%	HS inlet is opened completely

shows the pressure distributions of the bottom wall with 68% of throttle closed. The simulated results are similar to the experimental values. Thus, the fine grid has been adopted in the subsequent numerical investigations.



(a) mass flow rate of the HS inlet with varies backpressure at different transition stages



(b) the maximal pressure ratio at different transition stages

Fig. 3 Mass flow rate and the maximal pressure ratio of the HS inlet at different transition stages

3. Flow characteristic analysis of TBCC inlet mode transition

The unstart process lasts nearly several microseconds or even shorter (Wagner *et al.* 2009). While the process of the inlet mode transition is about several seconds. A large difference exists in the time scale between the two processes, inlet unstart occurs instantaneously with a certain backpressure and splitter position. Thus, it is reasonable to consider a steady state relationship between the inflow conditions (including the capture area) and the inlet states. Then the mode transition process is divided into five phases as shown in Table 1.

As we know, the primary purpose of an inlet is to capture and compress the airflow, maintaining a good performance of the engine (Zhao and Yi 2014, Luo *et al.* 2014). As the backpressure rises at the exit of the HS inlet, unstart shocks (or shock train) move forward. When the backpressure is extremely high, the shock train can be pushed out and no compression waves will exit in the isolator. Then, inlet unstart occurs together with a steep decrease of the mass flow. Take the Mach 2 case as an example, by 2-D steady numerical simulation the mass flow rates at

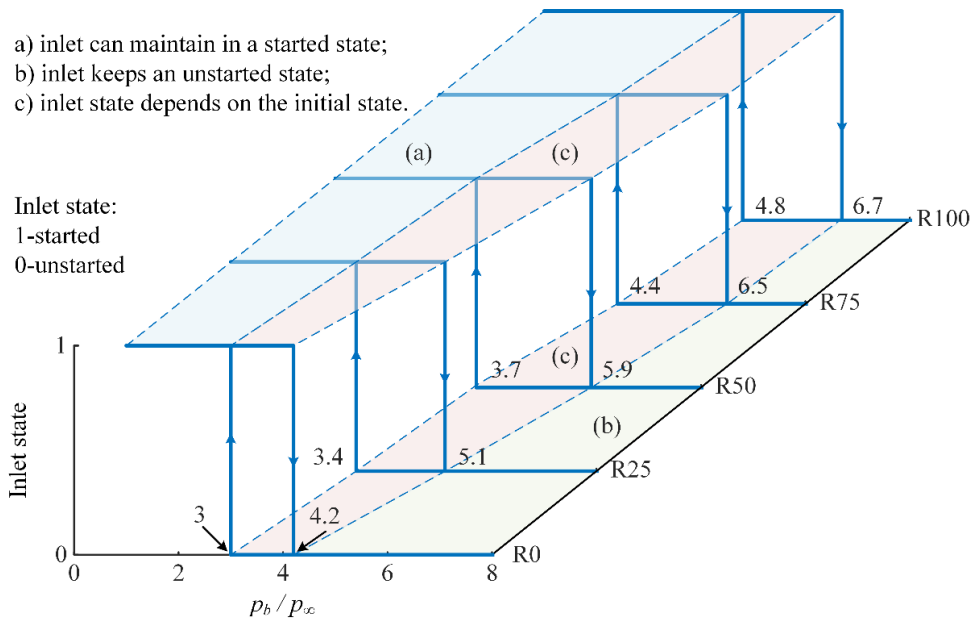


Fig. 4 Hysteresis of TBCC inlet mode transition at $M_\infty = 2.0$

each transition stage with different backpressure ratios can be obtained, which are shown in Fig. 5(a). At transition stage R0 (with the smallest internal contraction ratio), the mass flow rate is relative small and the shock train enters the bleeding region when the backpressure ratio reaches 3.5. As the backpressure continues to increase, the flow rate decreases rapidly but not so significantly. After the shock train passes through the bleeding region, a sharp decrease in the flow rate occurs, associate with the inlet unstart. With the transition process proceeding, the mass flow rate increases and the isolator can sustain a higher backpressure. Take the transition stage R100 as an example, the shock train will not across the bleeding region until the backpressure ratio reaches about 5.7. And the inlet unstart also occurs at a higher backpressure ratio. According to the relationship between the mass flow rates and backpressures, the unstart boundary can also be given as shown in Fig. 5(b), indicating that the maximum backpressure that HS inlet can suppress increases during the transition from LS inlet to HS inlet. Combined with the description of the mass flow rate, the poor performance of HS inlet in an unstarted state can be clearly displayed.

If the inlet is already unstarted, decreasing the backpressure to a certain value can make the inlet restart. Numerical simulations have been conducted with an initial fully unstarted state and the restart is achieved with a decreasing backpressure. In the same way, the restart boundary of the HS inlet is also obtained. Based on the simulation data of the inlet state with different backpressure ratios and transition stages, a description can be displayed in Fig. 6. The distinction between the unstart and restart pressure, leading to the hysteresis behavior, can be observed. And this phenomenon can be seen in each of the transition stage.

Take the transition stage R0 as an example, if the inlet is initial started and the inlet unstart will occur when the backpressure ratio reaches about 4.2. But decreasing the backpressure ratio from a higher value to 4.2 cannot make the inlet restart. Continue decreasing the backpressure ratio to 3, then the inlet restart occurs. The different control loops in transiting the inlet is described as a hysteresis loop. Extend these five hysteresis loops to the entire transition process, a hysteresis

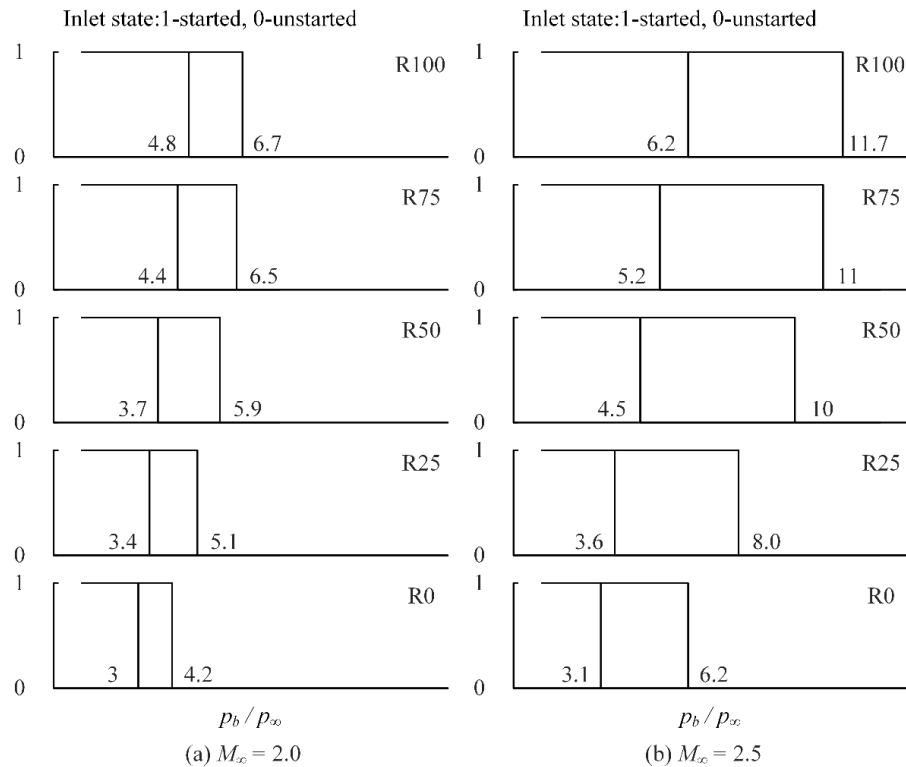


Fig. 5 A comparison of the hysteresis loops between $M_\infty = 2.0$ and $M_\infty = 2.5$

surface can be obtained. According to the description above, the hysteresis surface divides the operating space into three parts: in which a) inlet can maintain a started state; b) inlet keeps an unstarted state; c) inlet state depends on its initial state. As the operating space is linked with the hysteresis phenomenon, different control routes will result in disparate inlet states.

Meanwhile, we conducted the simulations with an incoming flow Mach number of 2.5 and the same scenario was also achieved. In Fig. 5 we report the comparisons of the hysteresis loops at $M_\infty = 2.0$ and $M_\infty = 2.5$. For a higher incoming Mach number, the inlet can suppress a higher backpressure. The unstart and restart backpressure ratios are both improved. From Fig. 5(a), we can observe that the width of the hysteresis loop increases with the inlet transition proceeding until it reaches R75. While the width of the hysteresis loop of stage R75 and R100 is nearly the same. The same result can also be observed at $M_\infty = 2.5$. And the hysteresis width at each transition stage is larger than that of $M_\infty = 2.0$.

4. Effect of the control route on unstart/restart characteristic

The hysteresis surface has been established based on the simulation results with a gap of 25% of the entire transition process. While for the verification cases, a gap of 20% are involved. Nine control routes have been designed as displayed in Table 2.

Fig. 6(a) gives a sketch of the control routes from 1 to 3. These control routes are all mapped on

Table 2 Control routes at $M_\infty = 2.0$

	R0	R20	R40	R60	R80	R100
Route 1	$2.0 p_\infty$	$2.4 p_\infty$	$2.8 p_\infty$	$3.2 p_\infty$	$3.6 p_\infty$	$4.0 p_\infty$
Route 2	$2.0 p_\infty$	$2.6 p_\infty$	$3.2 p_\infty$	$3.8 p_\infty$	$4.4 p_\infty$	$5.0 p_\infty$
Route 3	$2.0 p_\infty$	$3.2 p_\infty$	$4.4 p_\infty$	$5.6 p_\infty$	$6.8 p_\infty$	$8.0 p_\infty$
Route 4	$4.0 p_\infty$	$3.6 p_\infty$	$3.2 p_\infty$	$2.8 p_\infty$	$2.4 p_\infty$	$2.0 p_\infty$
Route 5	$4.0 p_\infty$	$4.4 p_\infty$	$4.8 p_\infty$	$5.2 p_\infty$	$5.6 p_\infty$	$6.0 p_\infty$
Route 6	$4.0 p_\infty$	$4.8 p_\infty$	$5.6 p_\infty$	$6.4 p_\infty$	$7.2 p_\infty$	$8.0 p_\infty$
Route 7	$6.0 p_\infty$	$5.2 p_\infty$	$4.4 p_\infty$	$3.6 p_\infty$	$2.8 p_\infty$	$2.0 p_\infty$
Route 8	$6.0 p_\infty$	$5.8 p_\infty$	$5.6 p_\infty$	$5.4 p_\infty$	$5.2 p_\infty$	$5.0 p_\infty$
Route 9	$6.0 p_\infty$	$2.0 p_\infty$				

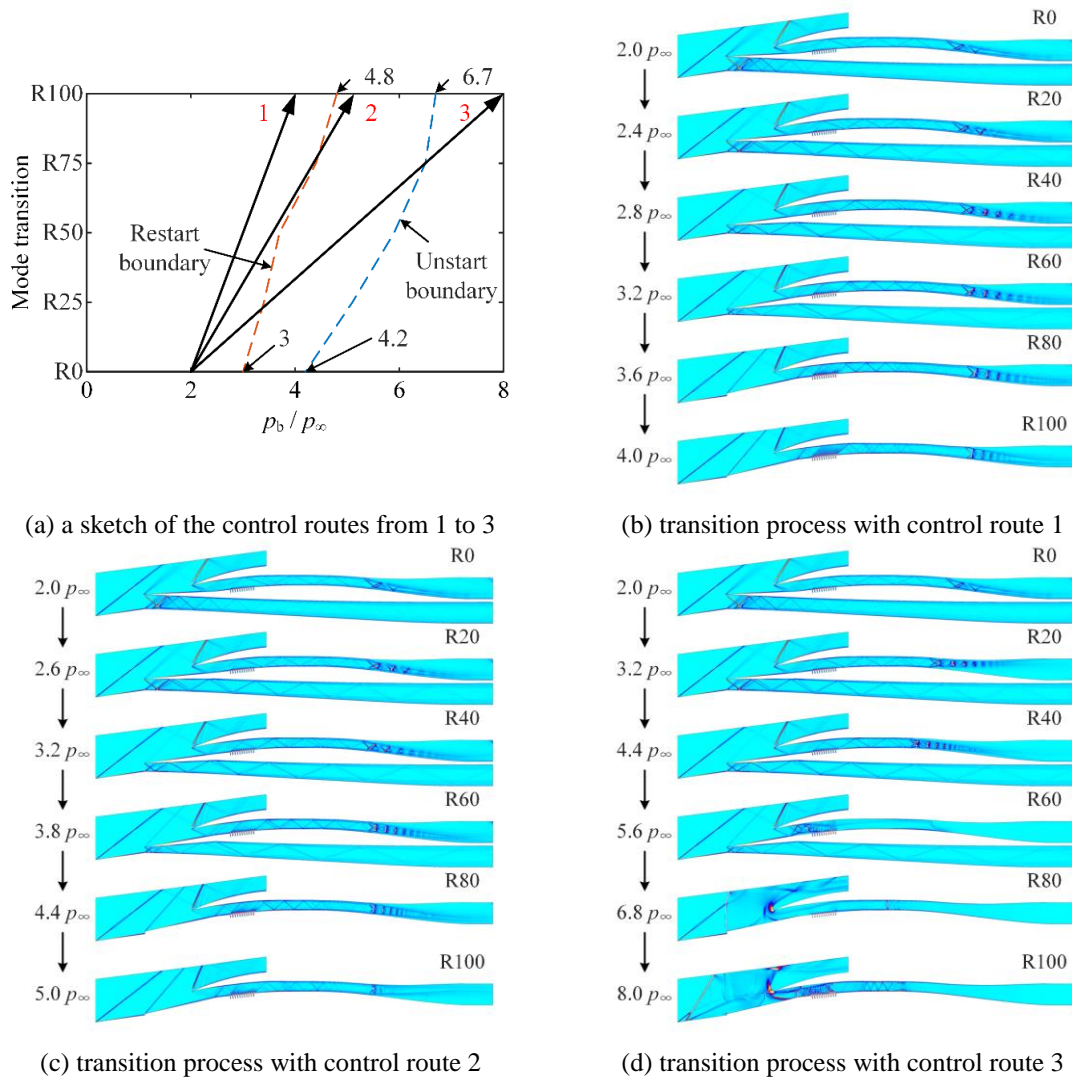


Fig. 6 Numerical Schlierens of the transition process with control route 1 to 3

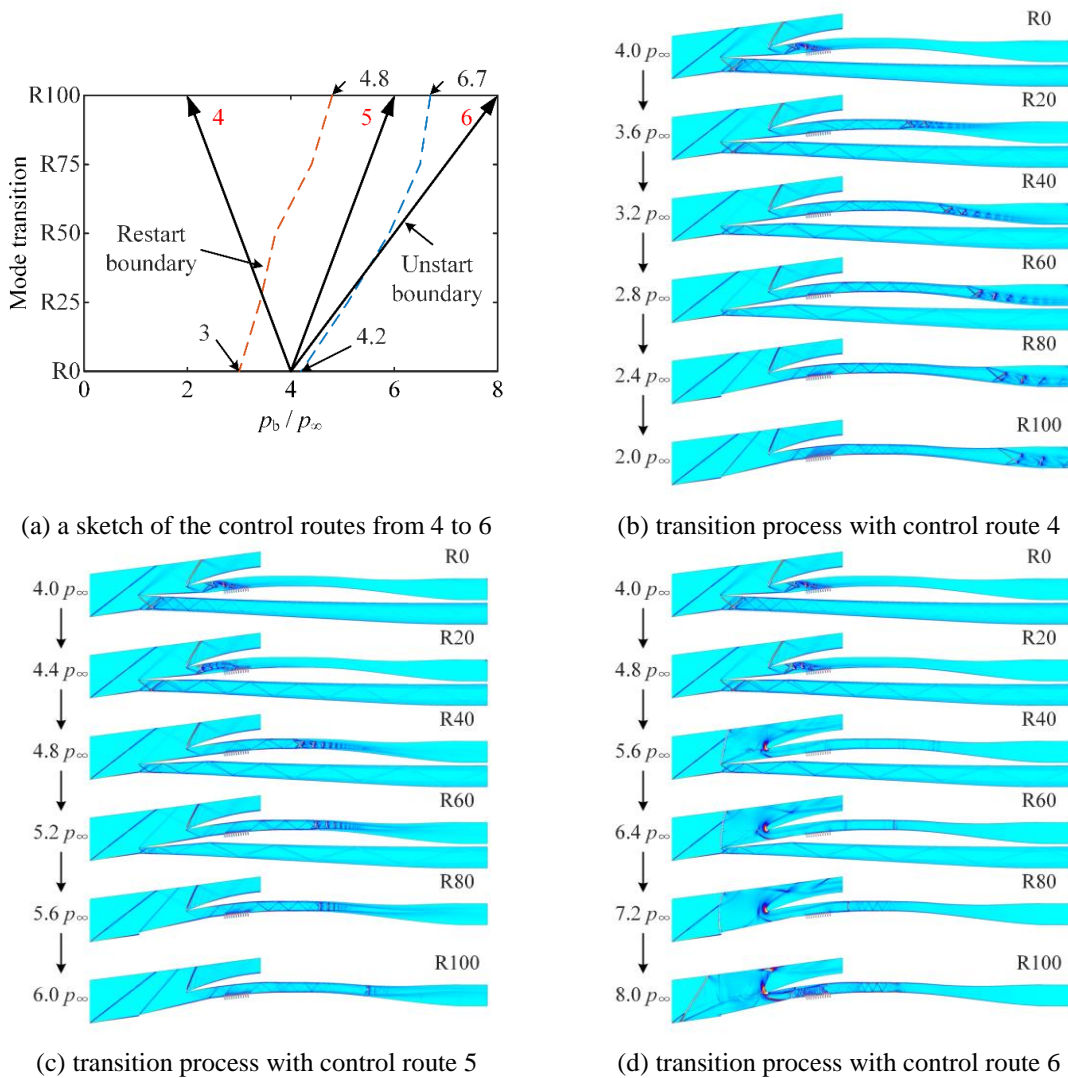


Fig. 7 Numerical Schlierens of the transition process with control route 4 to 6

the same horizontal plane. The verification cases for these three routes are all initialized with a fully started flow field. For route 1 and 2, the inlet transits from LS inlet to HS inlet with an increasing backpressure, but not crosses the unstart boundary. These two control routes are still within region (a) as labeled in Fig. 6, so inlet unstart will not occur. With the transition process proceeding, the inlet obtains a stronger ability of suppressing a higher backpressure. While for route 3, it crosses the unstart boundary during the transition and at R80 with a backpressure of $6.8 p_{\infty}$, inlet unstart occurs. The correlating numerical Schlierens are shown in Fig. 6(b)-(c).

Fig. 7(a) gives a sketch of the control routes from 4 to 6. The verification cases for these three routes are all initialized with a fully started flow field. For route 4, although HS inlet undergoes a relative high backpressure at the beginning, but with a decreasing backpressure the shock train moves backward and the inlet maintains a started state. For route 5, which has a same effect with

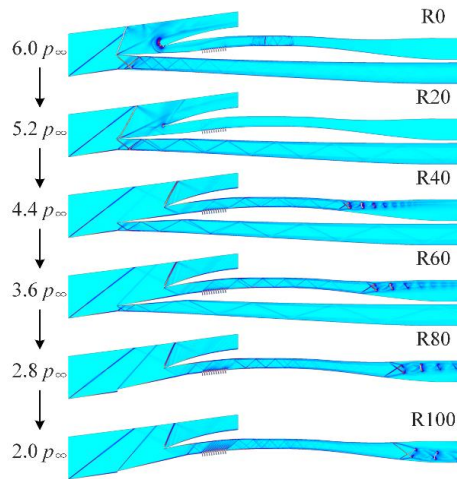


Fig. 8 Numerical Schlierens of the transition process under control route 4 with an unstarted initial state

route 1 or 2, it does not cross the unstart boundary, thus the inlet is still started. As for route 6, the inlet is operated towards the unstart boundary and achieves the same result with route 3. At transition stage R40 with a backpressure ratio of 5.6, which is already across the unstart boundary, the shock train is pushed out of the isolator. According to the numerical Schlierens as shown in Fig. 7(d), the separation induced shock spills the flow and with an increasing backpressure the separation is enhanced. Although a larger mass flow rate can be achieved with the splitter rotating downward, the backpressure is still beyond that the inlet can sustain.

The situation that the transition process with a fully started state is discussed above. While if the initial state is unstarted, the operation plane is switched to the lower part of the hysteresis surface (labeled by (c) in Fig. 6), which will lead to a disparate result. Take route 4 as an example (the inlet is operated towards the restart boundary), the increasing capture area together with the decreasing backpressure make the inlet restart again. The corresponding numerical Schlierens are shown in Fig. 8. We can notice the airflow spills out of the isolator largely at R0 with a backpressure ratio of 6.0. As the splitter rotates downward and the backpressure decreases, the spillage is reduced. As the transition goes on, the restart occurs between the stage of R20 and R40. For the other two routes, which operate the engine away from the restart boundary and the restart will never be achieved.

For routes 7 to 9, as shown in Fig. 9, the initial state of the inlet is unstarted. These routes are all within the lower part of the hysteresis surface. If the inlet operates along route 7, which will cross the restart boundary, the restart of the inlet can be achieved. According to the numerical Schlierens as shown in Fig. 9(b), the unstart shock at the entrance is inhaled into the isolator and the compression waves are constructed again. While for route 8 and 9, they never reach the restart boundary, thus the inlet maintains an unstarted state.

5. Conclusions

Numerical simulations have been conducted to investigate the unstart/restart characteristics of the TBCC inlet mode transition. The conclusions obtained in the present study can be summarized as below.

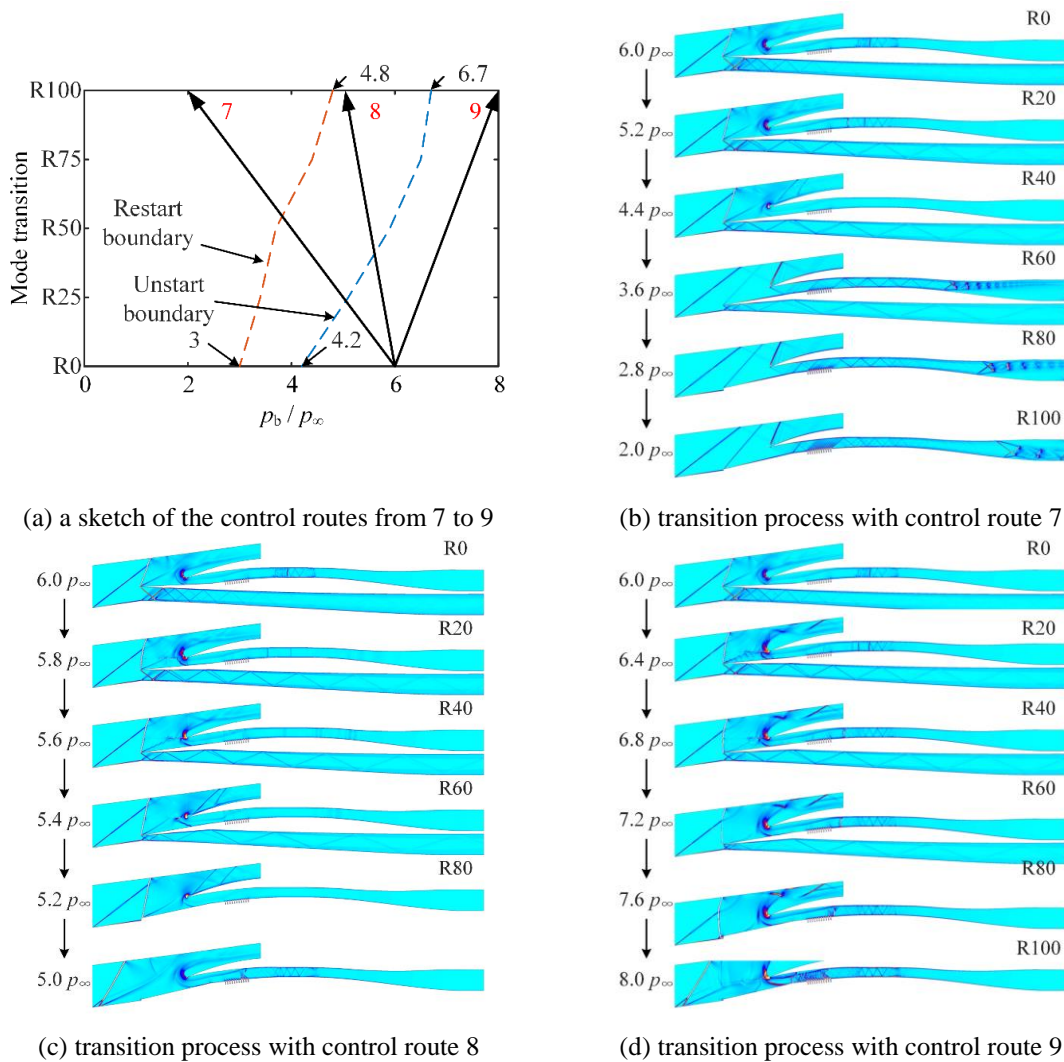


Fig. 9 Numerical Schlierens of the transition process under control route 7 to 9

- While the inlet transit from LS inlet to HS inlet (the splitter rotates from upside to downside), the maximum backpressure that the HS inlet can suppress increases with the transition process. And for a certain transition stage, the mass flow rate will not change significantly with the increasing backpressure in a started state. Once inlet unstart occurs, the mass flow rate decreases rapidly.

- The HS inlet undergoes a hysteresis behavior during the transition between start and unstart. At different transition stages, the width of the hysteresis loop is different. At a higher Mach number, the same scenario can be observed and the width of the hysteresis loop also increases. Based on the hysteresis loops at different stages, a hysteresis surface can be obtained, which separates the operating space of the engine into three parts.

- Nine control routes have been designed to verify the effect of the control route on the inlet unstart/restart characteristics. The control routes within the region which is not across the unstart

boundary will make the inlet maintain a started state. And also, the control routes within the region which is not across the restart boundary will make the inlet maintain an unstarted state. In the mutual region, the control routes with different initial conditions will result in disparate inlet states.

Acknowledgements

This research work is supported by the National Natural Science Foundation of China (Grants No. 51722601).

References

- Chang, J.T., Li, N., Xu, K.J., Bao, W. and Yu, D.R. (2017), "Recent research progress on unstart mechanism, detection and control of hypersonic inlet", *Prog. Aerosp. Sci.*, **89**, 1-22.
- Chang, J.T., Bao, W., Yu, D.R. and Shen, Y. (2009), "Effects of wall cooling on performance parameters of hypersonic inlets", *Acta Astron.*, **65**(3), 467-476.
- Cui, T., Lv, Z. and Yu, D.R. (2011), "Multistability and complex routes of supersonic inlet start/unstart", *J. Propul. Power*, **27**(6), 1204-1217.
- Cui, T., Tang, S.L., Zhang, C. and Yu, D.R. (2012), "Hysteresis phenomenon of mode transition in ramjet engines and its topological rule", *J. Propul. Power*, **28**(6), 1277-1284.
- Cui, T., Wang, Y. and Yu, D.R. (2014), "Bistability and hysteresis in a nonlinear dynamic model of shock motion", *J. Aircraft*, **51**(5), 1373-1379.
- Fu, C.G., Zeng, H., He, L.M., Sun, C.J. and Zhao, K. (2016), "Investigation on the influence of nozzle configuration on performance of a 2-stage PDE", *Acta Aerodyn. Sin.*, **34**(6), 770-777.
- Häberle, J. and Gülhan, A. (2008), "Investigation of two-dimensional scramjet inlet flowfield at Mach 7", *J. Propul. Power*, **24**(3), 446-459.
- Herrmann, C.D. and Koschel, W.W. (2002), "Experimental investigation of the internal compression of a hypersonic intake", *Proceedings of the 38th AIAA/ASME/SAE/ASEE Joint Propulsion Conference and Exhibit*, Indianapolis, U.S.A., July.
- Kantrowitz, A. and Donaldson, C. (1945), "Preliminary investigation of supersonic diffusers", NACA Rept. ACR-L5D20; Langley Memorial Aeronautical Laboratory, U.S.A.
- Kuzmin, A. (2015), "Shock Wave instability in a channel with an expansion corner", *J. App. Mech.*, **7**(2), 1-9.
- Kuzmin, A. (2016a), "Shock wave bifurcation in convergent-divergent channels of rectangular cross section", *Shock Waves*, **26**(6), 741-747.
- Kuzmin, A. (2016b), "Shock wave bifurcation in channels with a bend", *Arch. Appl. Mech.*, **86**(5), 787-795.
- Luo, J.L., Zhou, D., Kang, H.L. and Wang J.K. (2014), "Summarization of experimental methods associated with typical aerodynamic issues", *Acta Aerodyn. Sin.*, **32**(5), 600-609.
- Menter, F.R. (1994), "Two-equation eddy-viscosity turbulence models for engineering applications", *AIAA J.*, **32**(8), 1598-1605.
- Norris, G. (2011), "X-51A scramjet fails on second attempt", *Aerosp. Daily Defense Rep.*, **238**(55).
- Raj, N. and Venkatasubbaiah, K. (2012), "A new approach for the design of hypersonic scramjet inlets", *Phys. Fluids*, **24**(8), 86103.
- Saunders, J.D., Slater, J.W., Dippold, V., Lee, J., Sanders, B.W. and Weir, L.J. (2008), "Inlet mode transition screening test for a turbine-based combined-cycle propulsion system", *Joint Army-Navy-NASA-Air Force*, Boston, U.S.A., May.
- Taha, A.A., Tiwari, S.N. and Mohieldin, T.O. (2001), "Validation of fluent CFD code in supersonic flow fields", *Proceedings of the 15th AIAA Computational Fluid Dynamics Conference, Fluid Dynamics and*

- Co-located Conferences*, Anaheim, U.S.A., June.
- Voland, R.T. and Auslender, A.H. (1999), "CIAM/NASA Mach 6.5 scramjet flight and ground test", *Proceedings of the 9th AIAA International Space Planes and Hypersonic Systems and Technologies Conference*, Norfolk, U.S.A., November.
- Wagner, J.L., Yuceil, K.B., Valdivia, A., Clemens, N.T. and Dolling, D.S. (2009), "Experimental investigation of unstart in an inlet/isolator model in Mach 5 flow", *AIAA J.*, **47**(6), 1528-1542.
- Walker, S., Rodgers, F., Paull, A. and Van Wie, D.M. (2008), "HyCAUSE flight test program", *Proceedings of the 15th AIAA International Space Planes and Hypersonic Systems and Technologies Conference*, Dayton, U.S.A., April.
- Wang, D.P., Zhuang, Y., Tan, H.J., Zhang, H., Du, M.C. and Li, G.S. (2011), "Design and simulation of a dual-channel variable geometry turbine based combined inlet", *J. Aero. Power*, **11**(30), 2695-2704.
- Wilcox, D.C. (1994), *Turbulence modeling for CFD*, DCW Industries, CA, U.S.A.
- Zhao, H.Y. and Yi, M.R. (2014), "Review of design for forced-transition trip of hypersonic inlet", *Acta Aerodyn. Sin.*, **32**(5), 623-627.